Laminar flame speed determination at high pressure and temperature conditions for kinetic schemes assessment

F. Halter, G. Dayma, Z. Serinyel, P. Dagaut, C. Chauveau

Laminar flame speed determination at high pressure and temperature conditions for kinetic schemes assessment

1. **Author(s) and affiliation(s):**
   - F. Halter: CNRS-ICARE, Université d'Orléans, France
   - G. Dayma: CNRS-ICARE, Université d'Orléans, France
   - Z. Serinyel : CNRS-ICARE, Université d'Orléans, France
   - P. Dagaut : CNRS-ICARE, France
   - C. Chauveau: CNRS-ICARE, France

3. **Corresponding author:**
   - Fabien Halter
   - Mailing address: Institut de Combustion, Aérothermique, Réactivité et Environnement (ICARE), CNRS-INSIS, 1C Avenue de la Recherche Scientifique, 45071 Orléans Cedex 2, France
   - Email: fabien.halter@univ-orleans.fr

Abstract

Given the experimental difficulties, most of the available flame speed database is for relatively reduced thermodynamic conditions and for non-simultaneous variations of pressure and temperature. This limitation may be overpassed by using spherically expanding flames with the constant volume method. This methodology, introduced in the 30s by Lewis and von Elbe, requires the knowledge of the pressure evolution in the combustion chamber. It has been penalized for a long time because of the underlying assumptions and problems in flame instability detection. This method has been greatly renewed recently by Egolfopoulos following a coupled experimental/numerical approach integrating the effects of radiation and dissociation while maintaining moderate computing costs. In parallel with this study, we have worked on an alternative method providing a maximum of information for each test minimizing uncertainties. The current study uses a new experimental device allowing simultaneous recording of pressure and flame radius inside the chamber during the full combustion process. The direct use of these data over the whole flame propagation allows testing kinetic schemes over large pressure and temperature domains with good accuracy. These new experimental targets allowed the identification of key reactions needing improvements.

Keywords: Laminar flame speed; Flame kinetics; Engine conditions; Spherically expanding flame

1. Introduction

Flame speed is a sizing parameter to be considered in the design of energetic industrial systems such as IC engines [1, 2] and gas turbines [3]. Indeed, this physicochemical property of a combustible mixture notably affects the heat release rate such as the flame stabilization. Its significance makes it a major target for the validation of kinetic mechanisms. Because of experimental difficulties, most of the available flame speed database is for relatively reduced thermodynamic conditions and for non-simultaneous variations of pressure and temperature. This limitation may be greatly overpassed by using spherically expanding flames with the constant volume method [4]. This methodology, introduced in the 30s by Lewis and von Elbe [5], requires the knowledge of the pressure evolution in the combustion chamber.

Equations for this method have been the subject of several pioneered publications [6, 7]. Based on several assumptions (i.e. the pressure (P) is spatially uniform, the constituents of the burnt and unburnt gas behave as ideal gases, the unburnt gas is compressed isentropically), the following expression for the flame speed (S_u) was derived [8]:

$$S_u = \frac{dR_f}{dt} - \frac{\left(R_0^3 - R_f^3\right)}{3\gamma_u R_f^2 P}\frac{dP}{dt} \qquad (1)$$

where R_f and R_0 stand for the flame radius and the inner chamber radius and γ_u is the heat capacity ratio of the unburnt gas.

The isochoric method has been penalized for a long time because of the underlying assumptions (i.e. accuracy of the models for the burned mass fraction [9], stretch effects [10], influence of burnt gases equilibrium state [11] and of radiation [4]) and problems in flame instability detection [12]. This method has received particular attention in recent years [4, 10, 13-17].

The constant volume method relies on a spherical flame propagation until the walls. This criterion is relatively easy to achieve by designing a perfect spherical inner surface with an assembly of metal parts as done in [4, 14, 18] . However, compliance with this geometric constraint is hampered by the use of optical accesses with plane surfaces. Several chambers were developed to utilize both the flame front imaging (initial stages of propagation) and the pressure technique [16, 17, 19, 20]. In these studies, a specific attention was paid to the sphericity of the chamber. The following references report increasing windows to chamber diameters ratios. Hinton et al. [16] used a spherical vessel with a diameter of 160 mm and with one pair of windows (40 mm usable diameter) allowing to observe one fourth of the chamber. Groff [20] developed a 260 mm diameter chamber with two

opposed 92 mm diameter quartz windows. Omari and Tartakovski [17] designed a 1 L (Ø124.2 mm) spherical vessel, equipped on both sides with windows of 50.8 mm of diameter. This corresponds to 40% of the vessel diameter. Farrell et al. [19] used a 165 mm diameter spherical chamber with four windows. The two largest were 76 mm sapphire windows corresponding to slightly less than half of the chamber diameter. This latter study used, to the best of our knowledge, the almost spherical chamber with the largest windows to chamber diameter ratio.

However, one should keep in mind that when the flame front has travelled half the distance from the wall, the pressure has increased only by few percents as illustrated further in Figure 3. Clearly, these set-ups cannot afford simultaneous pressure and flame radius information necessary for the application of the isochoric method without resorting to a thermodynamic model.

Remarkable progress has been achieved with the derivation of clearly identified limits of data to process while guaranteeing negligible effects of stretch ($P/P_0 > 2$, with P_0 the initial pressure in the chamber), buoyancy ($S_u > 15\ cm/s$) and wall heat loss effects ($P/P_e < 0.75$, with P_e the theoretical end-pressure). Neglecting radiation heat loss when interpreting experimental data could lead to uncertainty as large as 15% as demonstrated in [4, 13]. This was limited by introducing radiation heat loss while keeping an inexpensive computational cost [4, 13, 21]. Meanwhile, we have developed an alternative method minimizing uncertainties using the isochoric method without resorting to any physical model [22]: A novel perfectly spherical isochoric combustion chamber with full optical access (OPTIPRIME), which allows the simultaneous recording of the pressure inside the chamber and of the flame radius evolution until the flame vanishes at the wall, making it fully innovative.

The current study brings new flame speed data for a large range of methane/air mixtures coupled with high pressure and temperature conditions (P_{max}~15 bar/ T_{max}~460 K). Literature mechanisms were used to simulate the data obtained in this study, showing important discrepancies.

2. Experimental Set up

The main novelty of the new combustion chamber lies in the 360° fused silica ring which allows a full radial visualization of the flame propagation until the walls. The spherical inner surface of this ring is in continuity with the inner chamber surface ($R_0 = 60.85\ mm$). As a result, the flame ignited in the chamber center, propagates outwardly in a perfectly spherical environment preventing any flame surface deformation. The pressure is monitored by the use of two pressure sensors (AVL GU21D) diametrically arranged. The chamber

is located in a furnace to ensure a homogeneous heating. The fresh gas temperature is controlled by a K-type thermocouple. A sketch of the experimental rig is presented in the supplementary materials (Figure a). More details about the description of the experimental set-up and the accuracy of the instruments are available in [22]. To ensure a perfect mixture repeatability, a high-pressure buffer tank (3.78 L) is filled with the components of the desire mixture following Dalton's law of partial pressures. The relatively large volume of the buffer tank, compared to the chamber volume (i.e. less than 1 L), allows carrying out successive shots tests at the three selected initial pressure conditions in this work ($P_0 = 1, 2\ and\ 3\ bar$). In the current study, the initial temperature (T_0) is kept constant at 300 K. Three equivalence ratios were selected: a fuel-lean mixture ($\Phi = 0.8$), a near-stoichiometric condition ($\Phi = 1.1$) and a fuel-rich mixture ($\Phi = 1.3$). Each mixture is sampled to confirm its composition by gas chromatography. The conditions tested in the current work are listed in Table 1. The theoretical end pressures considering adiabatic and isochoric combustion were evaluated using the CHEMKIN equilibrium calculator. Note that the ratio P_e/P_0 is independent of the initial pressure variation.

Table 1 : Initial mixture conditions tested.

Fuel	Oxidizer	T_0 (K)	P_0 (bar)	ϕ (-)	P_e (bar)
CH_4	Air	300	1 / 2 / 3	0.8	7.98 / 16.03 / 24.09
CH_4	Air	300	1 / 2 / 3	1.1	8.91 / 17.95 / 27.02
CH_4	Air	300	1 / 2 / 3	1.3	8.73 / 17.52 / 26.31

For each condition, at least three repetitions were performed. Repeatability was found to be excellent thanks to the careful determination of the initial conditions (mixture composition, initial temperature and pressure).

3. Results

3.1 Pressure and flame radius evolutions

Flame propagation was observed until the chamber walls through the 360° fused silica ring. For the current study, direct flame chemiluminescence visualization was adopted. The accurate flame front position determination using chemiluminescence through the ring was assessed in [22]. The acquisition rate of the CMOS camera (PHANTOM V1611) was set at 8000 fps for the fuel lean and rich conditions and 12 000 fps for the near-stoichiometric condition. The camera electronic shutter was set to the minimum value allowing a sufficient flame detection during propagation (i.e. < 10 µs for all flame conditions), ensuring that the flame front displaces for largely less than one pixel during this time. The resolution of the CMOS sensor was set to 1024x768 pixels^2 with a magnification ratio $\sigma = 0.124\ mm/pix$. Flame propagation visualization is illustrated

in Figure 1 for the fuel-rich atmospheric condition. The inner lateral spherical surface of the combustion chamber is delimited by the left and right red arcs. The ring allows a maximal vertical field of view of $50\ mm$. As illustrated in Figure 1, the flame visualization is possible until the flame reaches the wall. The plane in which the electrodes are located is tilted to be perpendicular to the viewing axis of the camera. For this condition, the flame remains perfectly spherical during the whole process, without the detection of any instability. The accuracy of the flame radius determination has been carefully assessed in [22]. The contributions of the different sources of inaccuracy were considered and precision on the flame radius of less than 0.5 % is attributed, as the pressure increases $\left(\frac{P}{P_0} > 2\right)$.

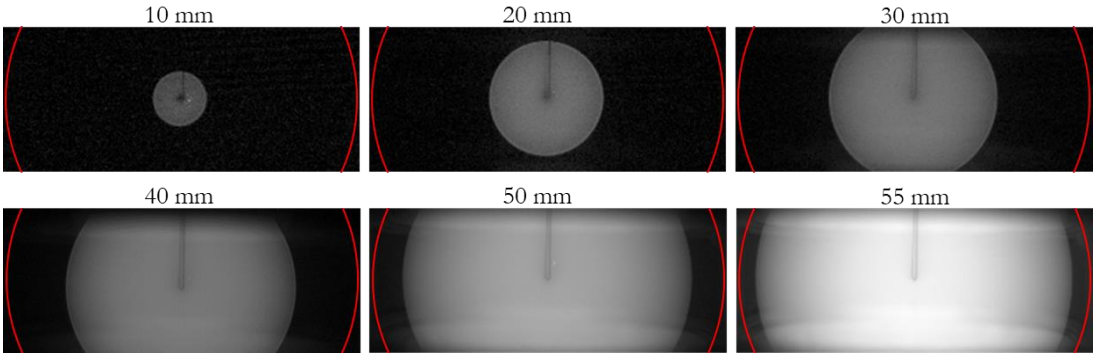

Figure 1 : Sequence of flame chemiluminescence visualization in the combustion chamber for flame radii ranging from 10 to 55 mm; CH_4/air flame ($\phi = 1.3$; $P_0 = 1\ bar$ & $T_0 = 300\ K$); Red contours indicate the inner diameter of the 360° quartz ring.

Pressure traces were acquired at a frequency of 20 kHz using two identical pressure transducers, connected to charge amplifiers linked to an acquisition system. The linearity of the sensor is ±0.3% of the full-scale range. The full scale was adapted for each pressure condition to optimize the precision leading to a maximal absolute error of $\pm 0.025\ bar$ for $P_0 = 1\ bar$ and $\pm 0.06\ bar$ for $P_0 = 3\ bar$. The two pressure traces are similar until the flame reaches the wall so only data of the top sensor are considered.

Pressure and flame radius signals, and their time derivatives, were filtered using zero-phase digital filtering to remove noise. Both the order of the filter and the range of data considered (minimal and maximal pressure) were systematically varied and adapted to each signal to ensure that this filter procedure does not affect the results. Pressure and flame radius evolutions are reported in Figure 2 for the atmospheric fuel lean mixture.

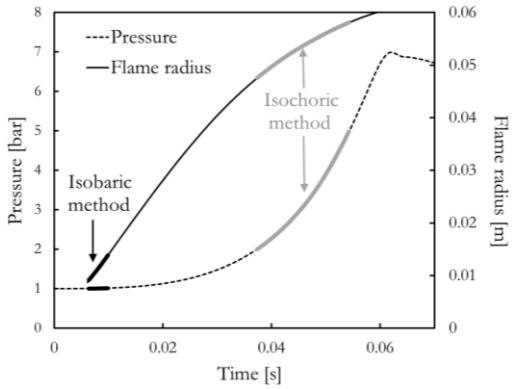

Figure 2: Pressure (dashed line) and flame radius (solid line) traces for the lean atmospheric CH4/Air mixture ($\phi = 0.8$; $P_0 = 1\ bar$ & $T_0 = 300\ K$). *Black/grey thick lines correspond to the data range considered for the isobaric/isochoric method.*

Pressure transducers and high-speed camera are both triggered at the ignition deposit. When the flame is close to the chamber walls ($R_f \rightarrow R_0$), the pressure evolution is affected by heat losses which prevent reaching the theoretical end pressure ($P_e = 7.98\ bar$ for this condition). The minimal flame radius detection is limited to 10 mm to avoid any disturbance from the ignition. The data range considered for the isobaric (black thick lines) and isochoric (grey thick lines) methods are specified in Figure 2. The isobaric method was limited to a maximal pressure elevation of less than 1 % of the initial pressure, corresponding to a maximal flame radius of less than 20 mm (i.e. less than 1/3 of the chamber radius). Traditionally, two metrics (i.e. laminar flame speed and burnt gas Markstein length) are extracted from the isobaric method. The isochoric method has the advantage to afford a large quantity of flame speed data for elevated pressure and temperature conditions. This method has been limited, for this illustration, to $2 < \frac{P}{P_0} < 5$ corresponding to $0.78 < \frac{R_f}{R_0} < 0.95$. The maximum pressure/radius to be considered for the flame speed evaluation should correspond to the adiabatic process. As explained in Omari et al. [17] and Burrell et al. [13], the time derivative of the pressure trace is a good indicator of the heat losses to the wall. In [22], a criterion of 90% of $max\left(\frac{dP}{dt}\right)$ was introduced to define the maximum experimental pressure to be considered in order to ensure that no wall effect can occur during the propagation investigated. Experimental traces of time pressure derivatives are plotted as a function of the dimensionless pressure in Figure 3 for the two extreme mixture conditions (black for $\phi = 0.8$ - grey for $\phi = 1.3$). For the fuel lean mixture condition, development of instabilities occurred during the flame propagation for initial pressures of 2 and 3 bar. The detection of instabilities by direct visualization or CH* chemiluminescence was illustrated in [22, 23] and the reader is referred to [22]. In Figure 3, unstable periods were colored in red. This method may help to detect the occurrence of instabilities for weakly stretched flames . For unstable flames, the curves exhibit a slight change of slope and the position of $max\left(\frac{dP}{dt}\right)$ is advanced. This information may be useful to detect the

occurrence of instabilities in the absence of optical access. For the near stoichiometric condition, not reported in Figure 3, flame instabilities also start to develop before the flame reaches the walls. In the rest of the work, flame speed evaluation will be limited to the stable regime for the fuel lean and near stoichiometric mixture conditions.

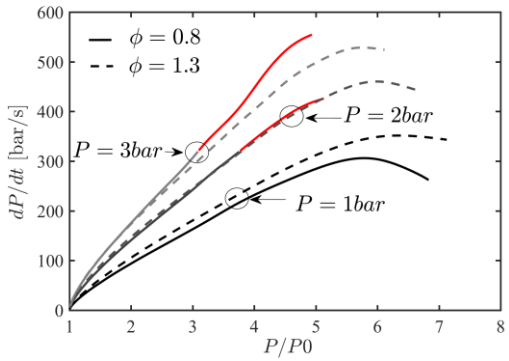

Figure 3 : Time derivative of pressure traces for lean (solid lines) and rich (dashed lines) CH_4/Air mixtures. Periods with unstable flames are indicated in red (occurring in the fuel lean condition). Black lines for 1 bar, dark gray for 2 bar and light gray for 3 bar.

With a criterion of 90% of $max\left(\frac{dP}{dt}\right)$, the maximal pressure to consider is estimated to be at least five times the initial pressure $(5.P_0)$ for all stable conditions. The position of $max\left(\frac{dP}{dt}\right)$ occurs for slightly lower P/P_0 when pressure is increased whereas, as indicated in Table 1, the ratio P_e/P_0 is almost independent of the initial pressure, keeping the initial temperature constant (i.e. $T_0 = 300\ K$). This would suggest that heat losses to the wall are more pronounced as initial pressure increases, which can be explained by the slowing down of the flame front and so an increase of the propagation and heat exchange times.

3.2 Flame speed evaluation

By design, OPTIPRIME provides, for each individual test, several major information on the flame dynamics: a) information on the occurrence of instabilities on the flame surface b) the laminar flame speed and the burned gas Markstein length are evaluated during the initial isobaric propagation c) the knowledge of the pressure and the flame radius traces allows evaluating the flame speed evolution for quite a large range of pressure and temperature conditions during the isentropic compression.

Isobaric method

Laminar flame speeds have been evaluated using the isobaric method and a nonlinear extrapolation as described in [24]. The high acquisition rates of the camera (8000 fps for $\phi = 0.8$ & $\phi = 1.3$ and 12 000 for $\phi = 1.1$) allowed obtaining at least 70 data points in the interval $10\ mm < R_f < 20\ mm$, keeping the relative pressure increase lower than 1 % in the chamber ($\frac{P}{P_0} < 1.01\ P_0$). Following the methodology proposed in Xiouris et al.

[4], the uncertainty quantification includes the contributions of: mixture preparation, data acquisition, and data processing. The mixture preparation is double-checked using chromatography analysis which significantly reduces its contribution. The uncertainty in the flame radius has been evaluated as lower than 1 pixel as in Halter et al. [22]. Data processing includes derivative evaluation and extrapolation to zero stretch. This results approximatively in a 1 cm/s absolute global error on the flame speed. Flame speeds evaluated with the isobaric method are reported by single symbols in Figure 4 and will be discussed in the next paragraph.

Isochoric method

Flame speed evolutions have been evaluated using Eq. (1). They are reported in Figure 4 along with the simulations performed using selected kinetic mechanisms (Table 2). Experimental traces range between $2 < \frac{P}{P_0} < 5$ which guarantees both negligible stretch effect [25] and heat loss to the walls. Flame speed evaluation is limited to stable regimes for $\phi = 0.8$ and $\phi = 1.1$.

Table 2 : Main features of the tested kinetic mechanisms

Mechanism	Species	Reactions
GRIMech 3.0 [26]	53	325
FFCM-1 [27]	38	291
HP Mech [28]	92	625
Aramco 1.3 [29]	253	1542

As done in [30], a relative accuracy of less than 0.5 % on the flame radius was propagated on the flame speed leading to a maximal error lower than 5%. The shot-to-shot variability is negligible compared to this maximal error of ± 5 %. Flame speed traces have been thickened to account for this uncertainty.

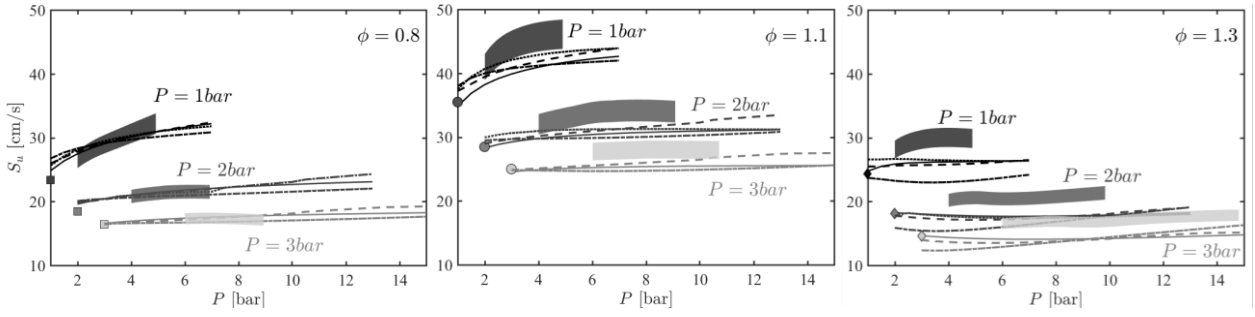

Figure 4 : Flame speed evolutions as a function of pressure for $\phi = 0.8$ (left), $\phi = 1.1$ (middle) and $\phi = 1.3$ (right). Thickened traces correspond to experimental results with their associated uncertainty (± 5 %). Single symbols are for isobaric results. Lines correspond to numerical results: Solid lines: FFCM-1 [27] - Dashed lines: HPMech [28] - Dot lines: ARAMCO 1.3 [29] - Dot-dashed lines: GRIMech 3.0 [26].

Laminar flame speeds determined using the isobaric period are reported in Figure 4 with single symbols (squares for $\phi = 0.8$, circles for $\phi = 1.1$ and diamonds for $\phi = 1.3$). Isochoric flame speed traces (thickened traces) extrapolated fairly well toward the isobaric values for all conditions. In this figure, data are colored according

to the initial pressure condition as well as the numerical results. Assuming isentropic compression (as validated in [4]), both pressure and temperature are increased during the flame propagation with the fresh gas temperature evolving as a function of $\left(\frac{P}{P_0}\right)^{(\gamma_u-1)/\gamma_u}$. Keeping the same pressure range for all conditions $\left(2 < \frac{P}{P_0} < 5\right)$ allows quasi-identical fresh gas temperature variations as the heat capacity ratio of the unburnt gas remains almost unchanged ($\sim 360\ K < T < \sim 460\ K$). For methane/air flame, pressure and temperature effects on flame speed have been widely characterized [31] and are generally modeled using power law formulations which express weak negative pressure and strong positive temperature dependences. The isentropic compression induces an absolute temperature variation of $100\ K$ in the considered pressure range $\left(2 < \frac{P}{P_0} < 5\right)$ whereas the absolute pressure variation is proportional to the initial pressure (3, 6 and 9 bar for 1, 2 and 3 bar respectively). These different absolute variations explain the different trends observed in Figure 4: Flame speed traces are increasing for the atmospheric condition whereas they are almost constant for higher initial pressure conditions. As already mentioned, an identical $\frac{P}{P_0}$ value corresponds to almost similar fresh gas temperature. As a result, plotting flame speeds as a function of $\frac{P}{P_0}$ allows isolating pressure effect on the flame speed.

Numerical method

The kinetic mechanisms used for simulations have been widely validated against data obtained under similar pressure and temperature conditions. Steady 1D simulations using the PREMIX package [32] from CHEMKIN-PRO software. Laminar burning velocities were calculated selecting multicomponent transport (MULT) and thermal diffusion (TDIF) with the same conditions of gradient and curvature (GRAD = 0.01 and CURV = 0.01) resulting in a similar number of meshes for each mechanism (> 1200). Thus, calculated laminar burning velocities vary by less than 1% between the last two calculation steps. For each condition of equivalence ratio and initial pressure, calculations were performed by steps of 0.5 bar, evaluating the corresponding initial temperature from the thermodynamic data assuming an isentropic compression. The ratio between isobaric and isochoric heat capacities of the fresh gases, γ_u, was evaluated for each calculation from the initial composition by an iterative process accounting for the temperature.

As can be seen from Figure 4, discrepancies can be observed between mechanisms, when the pressure increases, and for rich mixtures. For the lean CH_4/Air mixture, numerical results are in good agreement with the experimental traces. Generally speaking, for the lean mixture, the different evolutions are well reproduced,

demonstrating the ability of kinetic mechanisms to reproduce the coupled effect of pressure and temperature increase on the flame speed for these conditions. For the two other mixture conditions ($\phi = 1.1$ and $\phi = 1.3$), numerical predictions globally underestimate flame speed evolutions. This underestimation is more pronounced when the initial pressure is 1 bar. For the fuel-lean condition, most of the selected kinetic mechanisms are well able to reproduce the isobaric results, these mechanisms are also in good agreement with the most recent data reported in the review paper of Konnov et al. [31].

The most important discrepancies appear at $\phi = 1.3$, regardless of the initial pressure. Kinetic mechanisms exhibit different trends: GRIMech 3.0 predicts a decrease flame speeds from $P_0 = 1\ bar$, whereas HP Mech and Aramco 1.3 remain mostly constant, and FFCM-1 predicts an increase flame speeds, but not to the extent shown by experimental data.

4. Discussion

Sensitivity analyses on the flow rate were performed in order to better understand the complex behavior of the flame speed as a function of equivalence ratio, pressure and temperature. FFCM-1 was selected for these analyses as it gives reasonably good results compared to our experimental data, it has been validated over a large data set, and it converges remarkably well. Figure 5 presents four sensitivity analyses performed at $\phi = 0.8$ and $\phi = 1.3$, and at $P_0 = 1$ bar and 3 bar. Reactions were kept on this figure only if their sensitivity coefficient towards the flow rate was above 10%, i.e. 100% uncertainty on the rate constant involves 10% shift on the flame speed.

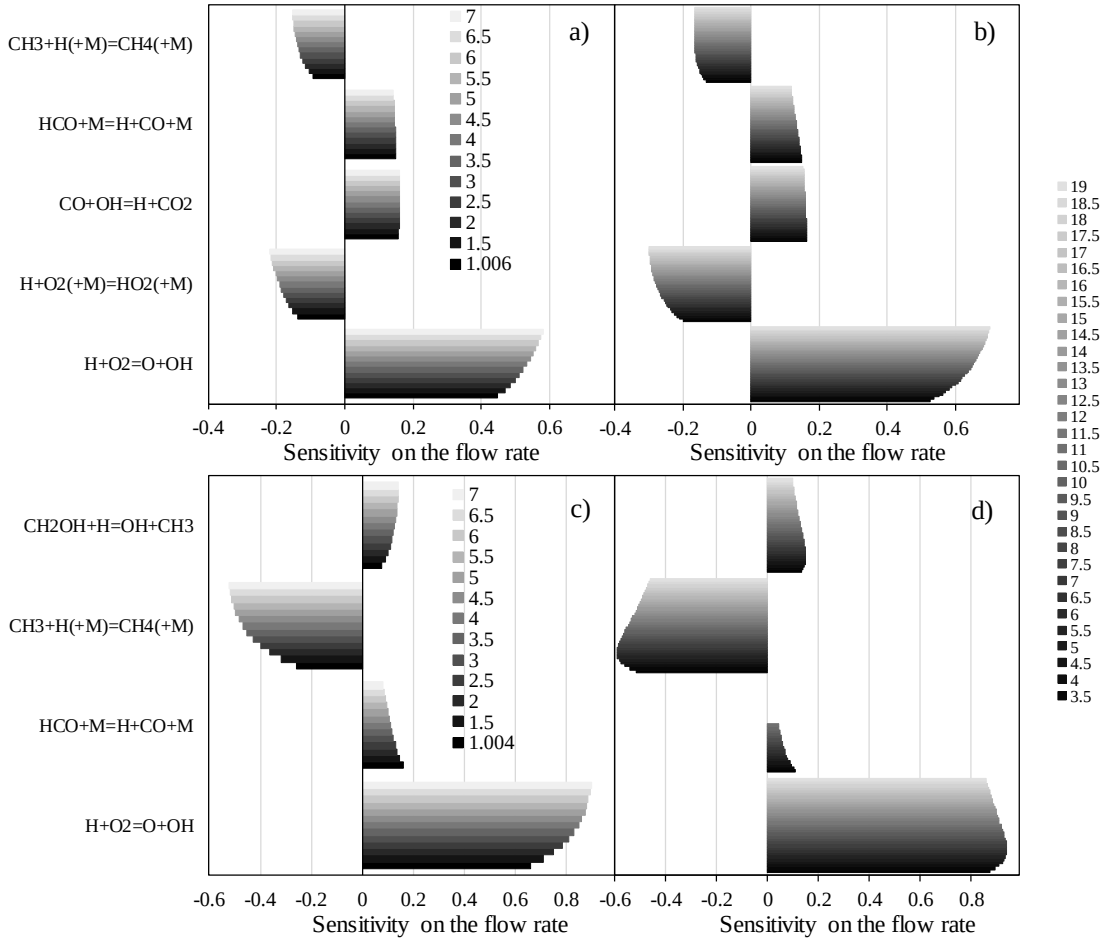

Figure 5: Sensitivity analyses on the flow rate for (a) $\phi = 0.8$ / $P_0 = 1$ bar, (b) $\phi = 0.8$ / $P_0 = 3$ bar, (c) $\phi = 1.3$ / $P_0 = 1$ bar, and (d) $\phi = 1.3$ / $P_0 = 3$ bar. The gray scale represents the evolution of the pressure in bar (the darker being the lower pressure as detailed in the legends).

Under fuel-lean conditions, (a) and (b), there are five highly sensitive reactions regardless of the initial pressure, H+O_2=O+OH being the most sensitive. The sensitivity of this branching step increases with pressure and temperature as does the sensitivity of its competitive reaction, namely H+O_2(+M)=HO_2(+M). The sensitivity of CO+OH=CO_2+H remains constant whereas the sensitivity of the decomposition of formyl radicals (HCO) slightly decreases when the pressure and temperature increase, as can be expected from a thermo-molecular reaction in the backward direction. Finally, the sensitivity of CH_3+H(+M)=CH_4(+M) increases with pressure before reaching a plateau above 10 bar and 416 K. It appears that, under these conditions, the flame speed evolution as a function of pressure and temperature is mainly driven by the evolution of the branching ratio between H+O_2=O+OH and H+O_2(+M)=HO_2(+M).

Under fuel-rich conditions ($\phi = 1.3$), (c) and (d), only four reactions exceed the set criterion. The sensitivity of H+O_2(+M)=HO_2(+M) went down the limit, as well as the sensitivity of the highly exothermic CO+OH=CO_2+H. The sensitivity of HCO+M=H+CO+M is similar to the fuel-lean case although more pressure- and temperature-dependent. Again, H+O_2=O+OH is the most sensitive reaction, an increase of which increases the flame speed.

Here, its competitive reaction in terms of H atoms consumption is CH_3+H(+M)=CH_4(+M), the sensitivity of which increases with pressure and temperature when $P_0 = 1$ bar. An interesting behavior appears when $P_0 = 3$ bar: the sensitivity of H+O_2=O+OH increases until the pressure reaches 7 bar ($T = 383$ K), then it decreases while the pressure and temperature keep increasing as the flame propagates. In the meantime, the sensitivity of CH_3+H(+M)=CH_4(+M) also increases until $P = 6.5$ bar ($T = 376$ K), before decreasing sharply. The sensitivity of the recombination step increases more strongly than that of the branching step whereas the decrease of the sensitivity is less pronounced for the branching step than for the recombination. It makes the flame speed first decrease by 3.9% up to $P = 7$ bar, and then increase by 0.8% ($P = 15$ bar and $T = 465$ K) as the flame continues to propagate.

From these analyses, CH_3+H(+M)=CH_4(+M) appears to be a key step controlling the flame speed as the equivalence ratio increases. In FFCM-1, which is an optimized kinetic mechanism, the original rate constant of this reaction was taken from Golden [33] and modified during the optimization process. Indeed, k_∞ (high pressure limit) was decreased by 14.65%, k_0 (low pressure limit) was not modified, Troe parameters were not modified either. On the other hand, third body efficiencies were greatly modified, for example the efficiency of of N_2 was decreased from 1 to 0.59, as O_2. To better match the actual new experimental data, it would be necessary to further decrease the rate constant of CH_3+H(+M)=CH_4(+M) (of around 25 %), the uncertainty of which is reputed to be 100% as implemented in FFCM-1. The calculated flame speeds with the modified value of this reaction were added in the supplementary materials (SM1-Figure b).

These analyses highlight the need for an accurate determination of the rate constant of CH_3+H(+M)=CH_4(+M) to better capture the pressure and temperature dependence of the CH_4/Air flame speed when the equivalence ratio increases. It appears that fuel-rich conditions are less accurately modeled by the mechanisms mainly due to the CH3+H(+M)=CH4(+M) reaction, which has higher sensitivity for a rich mixture than a lean one given the abundance of CH3 radicals and H atoms in richer mixtures.

4. Conclusion

The current study describes a new experimental set-up consisting of a spherical chamber equipped with a 360° transparent ring. This system allows the simultaneous recording of the pressure inside the chamber and, fully innovative, of the flame radius until the wall. This unique system makes it possible to track the flame front evolution during the whole combustion process. The direct flame visualization is useful to ensure that the flame surface remains perfectly spherical, without being affected by instabilities or gravity effects. The flame sphericity being checked, both isobaric and isochoric methods may be applied for each individual combustion test. The isochoric method is applied in the range $2 < \frac{P}{P_0} < 5$ which allows limiting to negligible stretch effects and heat losses to the wall. The direct measurement of the coupled experimental information (P & R_f) avoids the use of a model for the burnt gas fraction. Flame speeds were evaluated using the Fiock and Marvin equation with an associated accuracy estimated to less than ± 5 % ; the principal source of uncertainty being associated with the flame radius evaluation (relative precision of less than ± 0.5 %).

The current study provides new flame speed results methane/air mixtures for a wide range of conditions: $\phi = 0.8 - 1.1 - 1.3$, high pressure and high temperature (P_{max}~15 bar/ T_{max}~460K). Experimental results were compared to calculated flame speeds with four different kinetic mechanisms. The use of the isochoric method allowed a direct comparison over a large range of elevated pressure and temperature conditions, which is extremely challenging for mechanisms. It appears that fuel-rich conditions are less accurately modeled by the mechanisms mainly due to the CH_3+H(+M)=CH_4(+M) reaction.

As a main conclusion, it was demonstrated that the new experimental set-up is very promising in providing data for unexplored conditions in order to constrain and validate kinetic mechanisms.

[1] R. Cracknell, A. Prakash, R. Head, Influence of Laminar Burning Velocity on Performance of Gasoline Engines, SAE International 2012-01-1742 (2012).
[2] T. Tahtouh, F. Halter, E. Samson, C. Mounaim-Rousselle, Effects of hydrogen addition under lean and diluted conditions on combustion characteristics and emissions in a spark-ignition engine, International Journal of Engine Research 12 (5) (2011) 466-483.
[3] T. Poinsot, Prediction and control of combustion instabilities in real engines, Proc. Combust. Inst 36 (2017) 1-28.
[4] C. Xiouris, T. Ye, J. Jayachandran, F.N. Egolfopoulos, Laminar flame speeds under engine-relevant conditions: Uncertainty quantification and minimization in spherically expanding flame experiments, Combust. Flame 163 (2016) 270-283.
[5] B. Lewis, G. von Elbe, The Recording of Pressure and Time Gas Explosions, J. Am. Chem. Soc. 55 (2) (1933) 504-507.
[6] B. Lewis, G. von Elbe, Combustion, Flames and Explosions of Gases, Academic Press, New York, 2nd edition (1961).
[7] D. Bradley, A. Mitcheson, Mathematical solutions for explosions in spherical vessels, Combust. Flame 26 (1976) 201-217.
[8] E.F. Fiock, C.F. Marvin, F.R. Caldwell, C.H. Roeder, Flame speeds and energy considerations for explosion in a spherical bomb, National advisory committee for aeronautics, Report No. 682 (1940).
[9] C.C.M. Luijten, E. Doosje, L.P.H. de Goey, Accurate analytical models for fractional pressure rise in constant volume combustion, Int. J. Therm. Sci. 48 (6) (2009) 1213-1222.
[10] M. Faghih, Z. Chen, The constant-volume propagating spherical flame method for laminar flame speed measurement, Sci. Bull. 61 (16) (2016) 1296-1310.
[11] C.C.M. Luijten, E. Doosje, J.A. van Oijen, L.P.H. de Goey, Impact of dissociation and end pressure on determination of laminar burning velocities in constant volume combustion, Int. J. Therm. Sci. 48 (6) (2009) 1206-1212.
[12] K. Eisazadeh-Far, A. Moghaddas, H. Metghalchi, J.C. Keck, The effect of diluent on flame structure and laminar burning speeds of JP-8/oxidizer/diluent premixed flames, Fuel 90 (4) (2011) 1476-1486.
[13] R.R. Burrell, J.L. Pagliaro, G.T. Linteris, Effects of stretch and thermal radiation on difluoromethane/air burning velocity measurements in constant volume spherically expanding flames, Proc. Combust. Inst 37 (3) (2019) 4231-4238.
[14] Y. Yamamoto, T. Tachibana, Burning velocities of dimethyl ether (DME)–nitrous oxide (N2O) mixtures, Fuel 217 (2018) 160-165.
[15] D. Razus, M. Mitu, V. Giurcan, C. Movileanu, D. Oancea, Methane-unconventional oxidant flames. Laminar burning velocities of nitrogen-diluted methane–N 2 O mixtures, Process Safety and Environmental Protection 114 (2018) 240-250.
[16] N. Hinton, R. Stone, R. Cracknell, Laminar burning velocity measurements in constant volume vessels – Reconciliation of flame front imaging and pressure rise methods, Fuel 211 (2018) 446-457.
[17] A. Omari, L. Tartakovsky, Measurement of the laminar burning velocity using the confined and unconfined spherical flame methods – A comparative analysis, Combust. Flame 168 (2016) 127-137.
[18] J.L. Pagliaro, G.T. Linteris, P.B. Sunderland, P.T. Baker, Combustion inhibition and enhancement of premixed methane–air flames by halon replacements, Combust. Flame 162 (1) (2015) 41-49.
[19] J.T. Farrell, R.J. Johnston, I.P. Androulakis, Molecular structure effects on laminar burning velocities at elevated temperature and pressure, SAE International 2004-10-25 (2004).
[20] E.G. Groff, The cellular nature of confined spherical propane-air flames, Combust. Flame 48 (1982) 51-62.
[21] J. Jayachandran, F.N. Egolfopoulos, Effect of unsteady pressure rise on flame propagation and near-cold-wall ignition, Proc. Combust. Inst 37 (2) (2019) 1639-1646.
[22] F. Halter, Z. Chen, G. Dayma, C. Bariki, Y. Wang, P. Dagaut, C. Chauveau, Development of an optically accessible apparatus to characterize the evolution of spherically expanding flames under constant volume conditions, Combust. Flame 212 (2020) 165-176.
[23] G. Renoux, F. Halter, C. Chauveau, Experimental study of the morphology of two-phase flame instabilities in microgravity, Atomization Sprays 28 (10) (2019) 915-929.

[24] F. Halter, T. Tahtouh, C. Mounaïm-Rousselle, Nonlinear effects of stretch on the flame front propagation, Combust. Flame 157 (10) (2010) 1825-1832.
[25] Z. Chen, M.P. Burke, Y. Ju, Effects of compression and stretch on the determination of laminar flame speeds using propagating spherical flames, Combust. Theor. Model. 13 (2) (2009) 343-364.
[26] G.P. Smith, D.M. Golden, M. Frenklach, N.W. Moriarty, B. Eiteneer, M. Goldenberg, C.T. Bowman, R.K. Hanson, S. Song, W.C. Gardiner, V.V. Lissianski, Z. Qin, (http://www.me.berkeley.edu/gri_mech/.
[27] G.P. Smith, Y. Tao, H. Wang, Foundational Fuel Chemistry Model Version 1.0 (FFCM-1), https://web.stanford.edu/group/haiwanglab/FFCM1, (2016).
[28] http://engine.princeton.edu/mechanism/HP-Mech.html.
[29] W.K. Metcalfe, S.M. Burke, S.S. Ahmed, H.J. Curran, A hierarchical and comparative kinetic modeling study of C1 - C2 hydrocarbon and oxygenated fuels, International Journal of Chemical Kinetics 45 (10) (2013) 638-675.
[30] F. Halter, Z. Chen, G. Dayma, C. Bariki, Y. Wang, P. Dagaut, C. Chauveau, Development of an optically accessible apparatus to characterize the evolution of spherically expanding flames under constant volume conditions, Combust. Flame in press.
[31] A.A. Konnov, A. Mohammad, V.R. Kishore, N.I. Kim, C. Prathap, S. Kumar, A comprehensive review of measurements and data analysis of laminar burning velocities for various fuel+air mixtures, Prog. Energy Combust. Sci. 68 (2018) 197-267.
[32] R.J. Kee, F.M. Rupley, J.A. Miller, Chemkin-II: a Fortran chemical kinetics package for the analysis of gas phase chemical kinetics, Report No. SAND89-8009B, Sandia National Laboratories (1989).
[33] D.M. Golden, Yet another look at the reaction CH3 + H + M = CH4 + M, International Journal of Chemical Kinetics 40 (6) (2008) 310-319.

Acknowledgements

We are thankful to the CNRS, the University of Orléans, and the French Government Program ”Investissements d’avenir” through the LABEX CAPRYSSES.

List of Figures:

List of Tables: